Journal of Geophysical Research: Solid Earth

Supporting Information for

Seismological Indicators of Geologically Inferred Fault Maturity

H. Guo[1], T. Lay[1], and E. E. Brodsky[1]

1Department of Earth & Planetary Sciences, University of California Santa Cruz, CA, USA

Contents of this file

Supplementary Text

Brief Description of Earthquakes in Order of Decreasing M_W

Figures S1 to S23

S1-S22: Surface rupture maps showing segmentation

S23: Distribution of p-values

SI References

Supplementary Text

The 3 November 2002 Denali Earthquake

The M_W 7.9 Denali earthquake in Alaska (Figure S1) produced 341 km of surface rupture on the Susitna Glacier, Denali, and Totschunda faults (Haeussler et al., 2004). Although the earthquake started on the Susitna Glacier which is determined to be a thrust fault, the main rupture is on the Denali fault which is a long, strike-slip fault with relatively large cumulative fault offset. Therefore, this event occurred on a mature fault system.

The 14 November 2001 Kunlun Earthquake

The Kunlun fault in east central Tibet, near the northern boundary of the Tibetan Plateau, extends ~1600 km along strike with high slip rate (Van Der Woerd et al., 2002). The total surface rupture length of the M_W 7.8 earthquake is ~430 km, which is the longest coseismic surface rupture recorded for a continental earthquake (Fu et al., 2005). Relatively simple fault traces and high cumulative offset make indicate that this fault is mature.

The 13 November 2016 Kaikōura Earthquake

The M_W 7.8 Kaikōura earthquake in New Zealand (Figure S2) ruptured across the northeastern part of the South Island. The complex surface rupture extended for approximately 165 km across the New Zealand plate boundary zone with more than 17 faults involved (Nicol et al., 2018), including many unmapped ones. Surface rupture clearly shows the intersection and bend of the fault traces. Due to the great variations in the distribution and the small cumulative offset of these faults, we consider this area to be immature.

The 24 September 2013 Balochistan Earthquake

The M_W 7.7 Balochistan earthquake (Figure S3) occurred in southern Pakistan and ruptured the Hoshab fault for ~200 km. Although the Hoshab fault had been mapped as a reverse fault, this event has dominantly left-lateral strike slip motion (Avouac et al., 2014; Barnhart et al., 2015). Although the cumulative strike-slip offset is estimated to be ~11 km from river drainages (Zinke et al., 2014), this measurement for the Chaman fault, a NS strike-slip fault connected with the northern end of the Hoshab fault, is ~460 km (Valdiya & Sanwal, 2017). Structurally mature strike-slip faults are thought to have less shallow slip deficit in the upper crust (Fialko et al., 2005). The surface rupture of this event is relatively simple with no geodetically observed shallow slip deficit and therefore, we follow the previous assessment by Zinke et al. (2014) to consider this fault as a mature fault system.

The 16 July 1990 Luzon Earthquake

The M_W 7.7 Luzon earthquake (Figure S4) has a surface rupture of at least 120 km along the left-lateral Philippine fault (Klinger, 2010). As the southern end of the rupture extended offshore, the total rupture length is uncertain. The strike of the surface rupture changed little along the propagation. No clear information on the cumulative offset of this region is documented, therefore, we estimated this measurement to be 40 to 100 km from the modelled slip rate and fault age by Barrier et al. (1991). This estimate by Klinger (2010) varies from 100 to 200 km

since the Miocene. In general, the Philippine fault has large total fault offset with no branches or large variations in azimuth and can be considered a mature fault.

The 17 August 1999 Izmit Earthquake

The M_W 7.6 Izmit earthquake (Figure S5) generated a total of 110 km of dextral surface rupture at the western end of the North Anatolian Fault Zone (Langridge et al., 2002). The NAFZ has little variation in strike angles for different segments and has relatively large cumulative fault offset estimated to be ~72 to 88 km (Sunal & Erturaç, 2012; Akbayram et al., 2016). Therefore, we consider this fault system to be mature.

The 28 September 2018 Palu Earthquake

The M_W 7.5 Palu earthquake occurred on an active strike-slip fault at the main plate boundary between the Makassar block and the North Sula block with geological offset estimated to be 120 to 250 km (Socquet et al., 2019). The large cumulative fault offset and the straight geological fault lines allow us consider this fault as mature (Natawidjaja et al., 2021). The northeast end of the surface rupture is thought to involve a less mature fault from the observed moderate deficit of slip near the surface (Socquet et al., 2019).

The 21 May 2021 Maduo Earthquake

The M_W 7.3 Maduo earthquake ruptured the internal Bayan Har Block in the central Tibetan Plateau and generated a ~154 km-long surface rupture (Ren et al., 2022). The earthquake activated on the Jiangcuo Fault, which is one of the eight subparallel left-lateral strike-slip faults that form a diffuse zone between the Eastern Kunlun Fault and the Ganzi-Yushu-Xianshuihe fault system (Yuan et al., 2022). This fault is a secondary fault with relatively low-activity and had not been well mapped in previous studies. Total fault offset of the Eastern Tibet is not well known so we estimate the cumulative fault offset of this region as a moderate value, much smaller than 150 km, the total offset for the Kunlun fault (Van Der Woerd et al., 2002). The shallow slip deficit of this event is measured to be 10% to 30 % (Yuan et al., 2022; Yue et al., 2022). We classify this fault as a mature to intermediate mature fault system.

The 28 June 1992 Landers Earthquake

The M_W 7.3 Landers earthquake (Figure S6) ruptured ~75 km along several right-lateral faults within the eastern California shear zone (ECSZ) (Klinger, 2010). Previous studies on this area have estimated the total offset across the ECSZ to be more than 40 km, whereas the cumulative strike-slip offset is ~4.6 km (Jachens et al., 2002). Considering the complex rupture traces and the moderate fault offset, we assess the Landers earthquake as occuring on a relatively immature or intermediate mature fault system.

The 10 May 1997 Zirkuh Earthquake

The M_W 7.2 Zirkuh earthquake (Figure S7) ruptured the northern part of the Abiz fault, which is the longest surface rupture in Iran and bounds the Luth block to the East. The total length of the surface rupture of this event is ~125 km (Ansari, 2021; Marchandon et al., 2018) with the cumulative offset for this region measured to be 70 to 105 km (Walker & Jackson, 2004). Ansari

(2021) suggested that the northern section of the Abiz fault has longer slip history without splay branches and is more mature than the southern section. However, considering there is no significant shallow slip deficit along the Abiz fault (Marchandon et al., 2018), we assess this fault system as mature.

The 12 November 1999 Düzce Earthquake

The M_W7.2 Duzce earthquake (Figure S8) occurred on the North Anatolia Fault Zone (NAFZ) with the rupture length estimated to be ~40 km (Duman et al., 2005). The NAFZ has relatively large cumulative fault offset of ~72 to 88 km (Sunal & Erturaç, 2012; Akbayram et al., 2016) so the event generated on a mature fault system.

The 14 August 2021 Nippes Earthquake:

The M_W 7.2 Nippes earthquake initiated on a blind thrust fault and then jumped onto a strike-slip fault propagating westward from the epicenter accommodated by a network of segmented faults with diverse faulting conditions (Okuwaki & Fan, 2022). The main strike-slip fault across this region is the Enriquillo-Plantain Garden Fault which is a left-lateral strike-slip fault that extends over ~1100 km. The measured cumulative fault offset measured is moderate which suggests this is a relatively immature fault system.

The 7 December 2015 Sarez Earthquake

The M_W 7.2 Sarez earthquake (Figure S9) reactivated a ~79 km section of the Sarez-Karakul fault while the surface ruptures extend discontinuously for 37 km (Elliott et al., 2020; Sangha et al., 2017). The fault lines do not have large variations in strike or complex branches. Although there is no clear measurement of the total offset along this fault, the determined displacement for the strike-slip systems of the Pamir can be as large as 300 km (Schmidt et al., 2011), which indicates a mature fault system in this region.

The 4 April 2010 El Mayor- Cucapah Earthquake

The M_W 7.2 El Mayor- Cucapah earthquake (Figure S10) in 2010 ruptured for ~120 km from the northern tip of the Gulf of California to the U.S.–Mexico border. No cumulative fault offset is measured in this region. However, studies have shown that these faults are likely to have low total slip with many distributed small faults. Therefore, we infer that the faults in this region are immature.

The 16 October 1999 Hector Mine Earthquake

The M_W 7.1 Hector Mine (Figure S11) earthquake has a ~48 km-long dextral surface rupture within the eastern California shear zone (ECSZ) including various branches and segments. ECSZ have long-term displacements ranging from 1.5 to 14.4 km and a net total slip of about 65 km (Treiman et al., 2002). Most of the faults ruptured during this earthquake had prior late-Quaternary displacement while the evidence for Holocene displacement is limited. We infer that these faults can be categorized as immature.

The 6 July 2019 Ridgecrest Earthquake

The two large events in the Ridgecrest sequence (Figure S12) that occurred in the central eastern California shear zone (ECSZ) are both included in this study. Surface ruptures of both the foreshock and the mainshock show many previously unmapped orthogonal faults. These distributed strike-slip faults are young and have modest cumulative fault offset and are inferred to be immature due to the complex faulting.

The 27 May 1995 Neftegorsk Earthquake

The M_W 7.1 Neftegorsk earthquake (Figure S13) ruptured ~46 km at the northern end of Sakhalin Island, which is considered to be an inactive plate boundary between the North American and Eurasian plates (Arefiev et al., 2000). Dextral motion of the southern part of the strike-slip zone is related to the inception of subduction at the Japan arc during late Miocene. Although the main rupture is straight, there are several strands distributed at the end of the rupture. Considering the moderate cumulative fault offset, we infer this fault is immature.

The 3 September 2010 Darfield Earthquake

The M_W 7.0 Darfield earthquake (Figure S14) in New Zealand occurred on a previously unidentified fault system and ruptured the surface for ~29.5 km (Quigley et al., 2012). Although the surface rupture shows moderate variation in strike angle, the earthquake propagated across a structurally complex fault network including optimally oriented faults (M. C. Quigley et al., 2019), which suggests an immature fault system. Cumulative fault offset of this region is currently unknown.

The 14 April 2016 Kumamoto Earthquake

The M_W 7.0 Kumamoto earthquake (Figure S15) ruptured ~40 km of the Futagawa-Hinagu Fault Zone (FHFZ) on Kyushu Island, Japan (Scott et al., 2019). FHFZ activated around 0.7–0.5 Ma and may have generated a moderate cumulative displacement. The rupture involved many strands or branches scattering in space and varying in strike angle. We infer that the FHFZ is an immature fault system.

The 12 January 2010 Haiti Earthquake

The M_W 7.0 Haiti earthquake ruptured an unmapped north-dipping fault named as Léogâne fault, which is parallel to the Enriquillo–Plantain Garden fault (EPGF), one of two main strike-slip faults between the Caribbean and North American plates (Calais et al., 2010). Moderate cumulative offset for the eastern EPGF indicates that faults of this region are immature. Aftershocks of this earthquake are mainly thrust events, which occurred on an activated structure dipping to the south which might explain the relatively high productivity ratio of this event.

The 12 February 2014 Yutian Earthquake

The M_W 6.9 Yutian earthquake (Figure S16) ruptured for ~45 km while the mapped surface rupture is only 25 km and involves a big stepover. Although the event ruptured the western edge of the Altyn Tagh Fault which is a mature fault with hundreds of kilometers of total offset, its nucleation occurred at the eastern end of the South Xiaoerkule Fault which is one of the parallel

faults caused by the eastward extrusion of the Tibetan terrane relative to the Tianshuihai block. Earthquakes generated at fault ends with large stepovers are usually immature.

The existence of the large stepover slows down the rupture velocity and the bilateral propagation includes more error in determining the rupture velocity. Therefore, we do not the relation between geological measurements and rupture velocity for this specific event.

The 13 April 2010 Yushu Earthquake

The M_W 6.9 Yushu earthquake (Figure S17) occurred on the Ganzi–Yushu fault, forming part of the Yushu–Ganzi–Xianshuihe fault zone which is one of the most active fault zones in eastern Tibet. The surface rupture is separated by some stepovers a few kilometers wide and by small azimuth changes (Li et al., 2012). The cumulative fault offset of this fault is estimated from river drainage systems to be tens of kilometers. We assume this fault system is mature.

The 24 March 2011 Tarlay Earthquake

The M_W 6.8 Tarlay earthquake ruptured for ~30 km along the westernmost section of the left-lateral Nam Ma fault, Myanmar, with the coseismic surface rupture extending more than 17 km (Wang et al., 2014). The fault line is relatively straight without big bends or branches. However, the rupture occurred at the end of a fault with apparent shallow slip deficit and the relatively small cumulative fault offset indicates that this fault system is immature.

The 24 January 2020 Sivrice Earthquake

The M_W 6.7 Sivrice earthquake is the first earthquake providing rupture details of the East Anatolian Fault Zone (EAFZ) which is a major continental strike-slip fault between the Arabia plate and the Anatolian Block. Although no clear surface rupture was documented, small cracks occurred along a 48 km-long region (Çetin et al., 2020). This EAFZ event has significant slip deficit and a moderate total slip, which indicate that the EAFZ is likely to be an immature fault system.

The 26 December 2003 Bam Earthquake

The M_W 6.6 Bam earthquake occurred on a newly mapped fault at the southern end of the Nayband and Sarvestan fault located in western Dasht-e-Lut. There are no direct surface faulting features associated with this earthquake, but it produced some surface cracks which extend along a region with total length of 22.5 km (Maleki Asayesh et al., 2020). This fault system may be young and immature, accommodating reverse and strike-slip components of oblique convergence across the zone.

The 24 November 1987 Superstition Hills Earthquake

The M_W 6.6 Superstition Hills earthquake (Figure S18) ruptured a ~26 km-long section at the southern part of the right-lateral San Jacinto fault system with significant afterslip (Klinger, 2010). The cumulative offset along the Superstition Hills Fault is not well documented. The estimated moderate value indicates a fairly immature fault system.

The 31 March 2020 Stanley Earthquake

The M_W 6.5 Stanley earthquake occurred in the southern part of the Northern Rocky Mountains province, which is characterized by several active normal faults that have produced Pleistocene to Holocene ruptures. This event initiated on an unmapped strike-slip fault and traversed a 10-km-wide (at the surface) stepover. We infer that this new formed fault system is an immature one.

The 8 August 2017 Jiuzhaigou Earthquake

The M_W 6.5 Jiuzhaigou earthquake occurred on an unknown fault at the southern branch of Tazang Fault which is one of the tail structures at the easternmost Kunlun fault zone. This event has no surface rupture zones with a buried fault strand of the unmapped northern extension of the Huya fault with strong shallow slip deficit, which may reflect immaturity of this fault zone.

The 15 May 2020 Monte Cristo Range Earthquake

The M_W 6.5 Monte Cristo Range earthquake ruptured a previously unidentified fault system in the easternmost central Walker Lane Belt (WLB) which defines a complex shear zone in the Pacific-North America plate boundary. The rupture of this earthquake is segmented without prior mapped Quaternary faulting and has modest surface break, which indicates a relatively immature fault system that has not accumulated significant total slip.

The 4 July 2019 Ridgecrest Foreshock

The M_W 6.4 foreshock in the Ridgecrest sequence (Figure S19) occurred in the central eastern California shear zone (ECSZ). Surface ruptures of the foreshock and mainshock show many previously unmapped orthogonal faults. These distributed strike-slip faults are young and have very small cumulative fault offset and are inferred to be immature due to the complex faulting.

The 29 December 2020 Petrinja Earthquake

The M_W 6.4 Petrinja earthquake has a ~13 km-long rupture at conjugate faults dominated by the active Pokuplje Fault associated with the motion between Adria and the Eurasian Plate. Total offset of this fault system is few which suggests that the fault is immature.

The 15 October 1979 Imperial Valley Earthquake

The M_W 6.4 Imperial Valley earthquake (Figure S20) is the oldest event utilized in this study and ruptured ~30 km along the northern section of the Imperial fault at the US-Mexico border. The Imperial fault has the same slip rate as the San Jacinto fault with moderate cumulative fault slip (Lindsey & Fialko, 2016; Powers & Jordan, 2010; Stirling et al., 1996) and can be characterized as a relatively immature fault system.

The 24 August 2014 Napa Earthquake

The M_W 6.0 South Napa earthquake (Figure S21) occurred in the San Francisco Bay Area and produced a 12 km long surface rupture with right-lateral strike-slip displacement. The East Bay fault system has a relatively large right-lateral offset. Although there are many small fault lines

in the surface rupture, they are short compared to the main rupture and may not represent the fault distribution properly. We infer that the fault system in this region is moderately mature.

The 28 September 2004 Parkfield Earthquake

The M_W 6.0 Parkfield earthquake on the central San Andreas Fault has been documented to have large total offset at around 315 km. Surface rupture of this event is clear and straight without distributed branches. Therefore, this event occurred on a mature fault system.

Figures

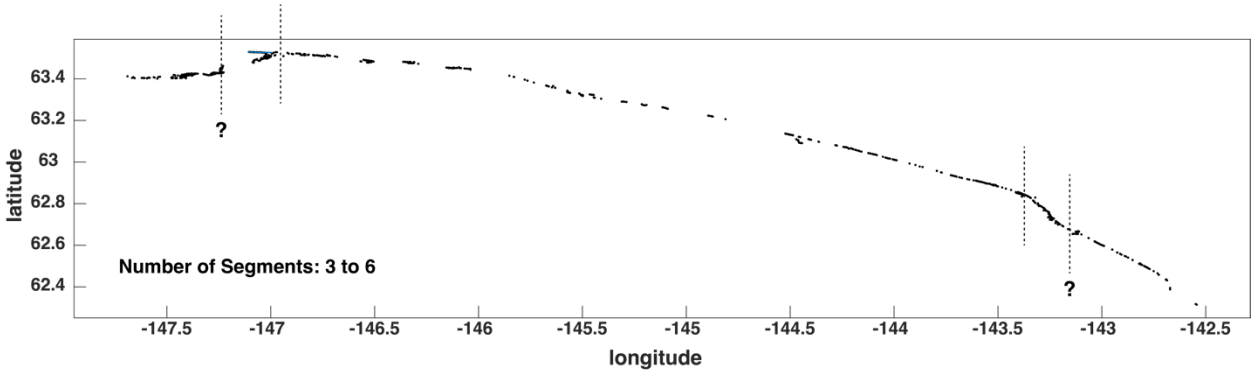

Figure S1. Surface rupture and segmentation results for the Denali earthquake. Dashed lines present the possible segment limits. Those with question markers are alternative possibilities that are uncertain.

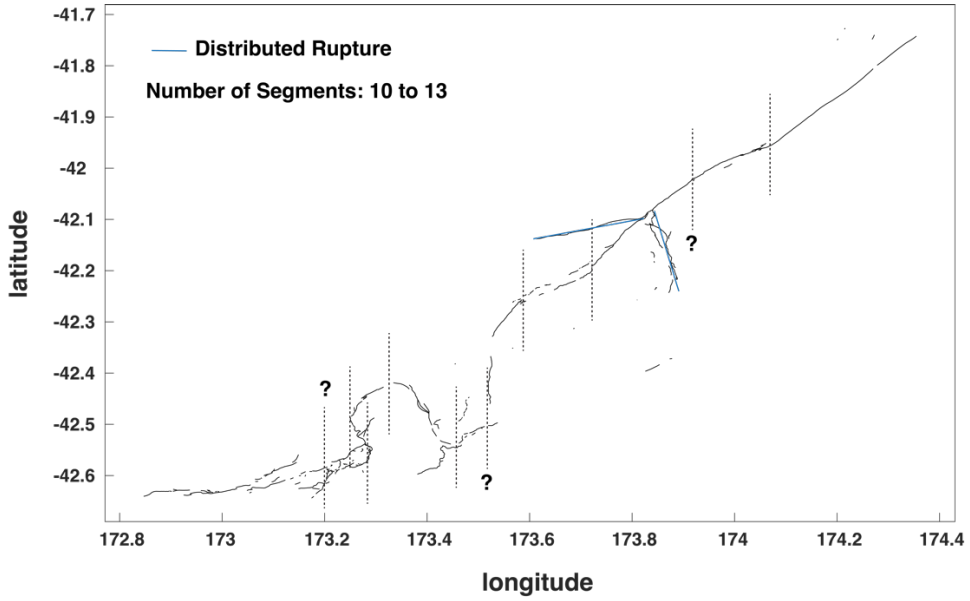

Figure S2. Surface rupture and segmentation results for the Kaikoura earthquake.

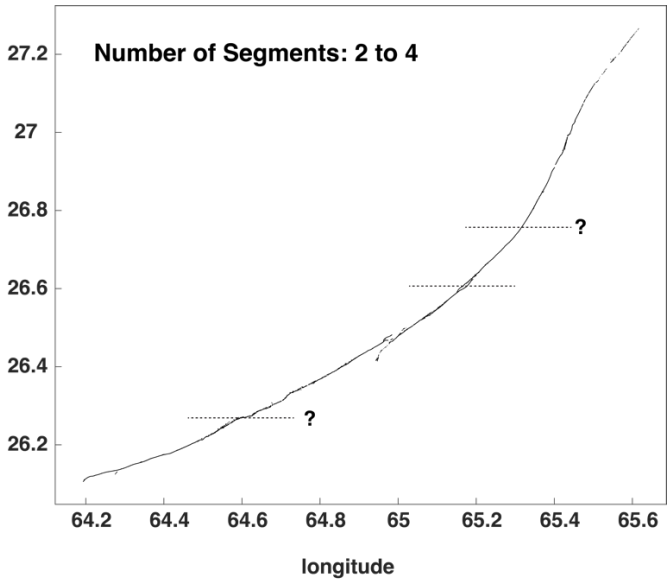

Figure S3. Surface rupture and segmentation results for the Balochistan earthquake.

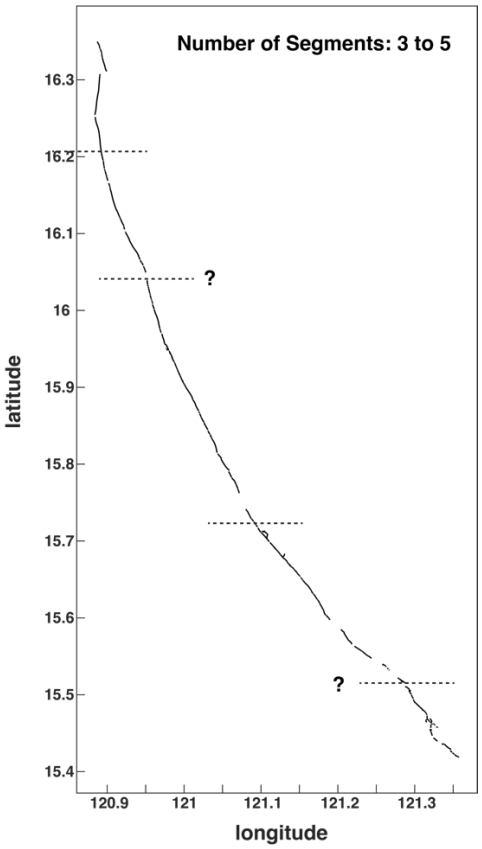

Figure S4. Surface rupture and segmentation results for the Luzon earthquake.

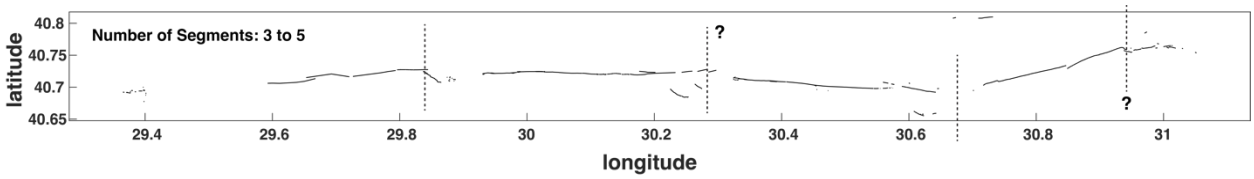

Figure S5. Surface rupture and segmentation results for the Izmit earthquake.

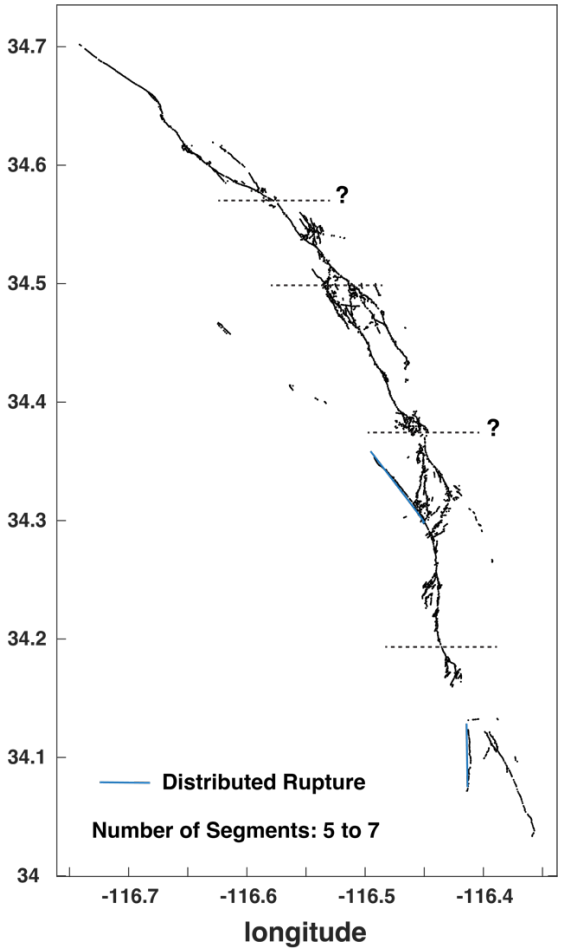

Figure S6. Surface rupture and segmentation results for the Landers earthquake.

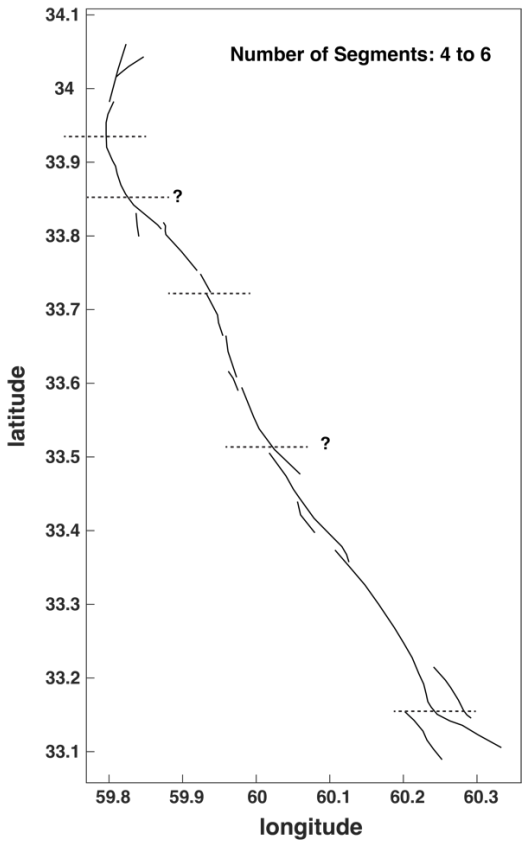

Figure S7. Surface rupture and segmentation results for the Zirkuh earthquake.

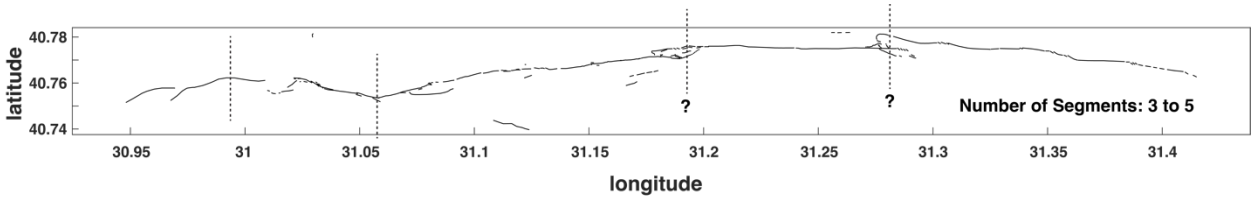

Figure S8. Surface rupture and segmentation results for the Düzce earthquake.

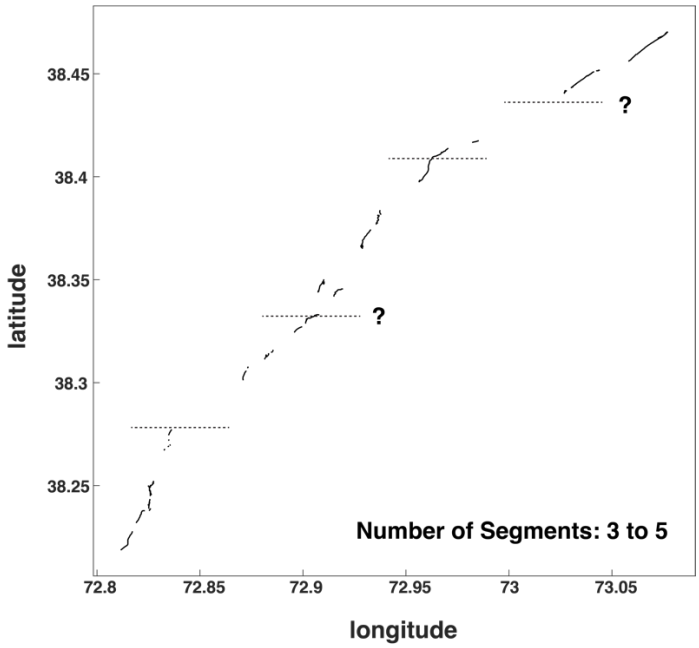

Figure S9. Surface rupture and segmentation results for the Sarez earthquake.

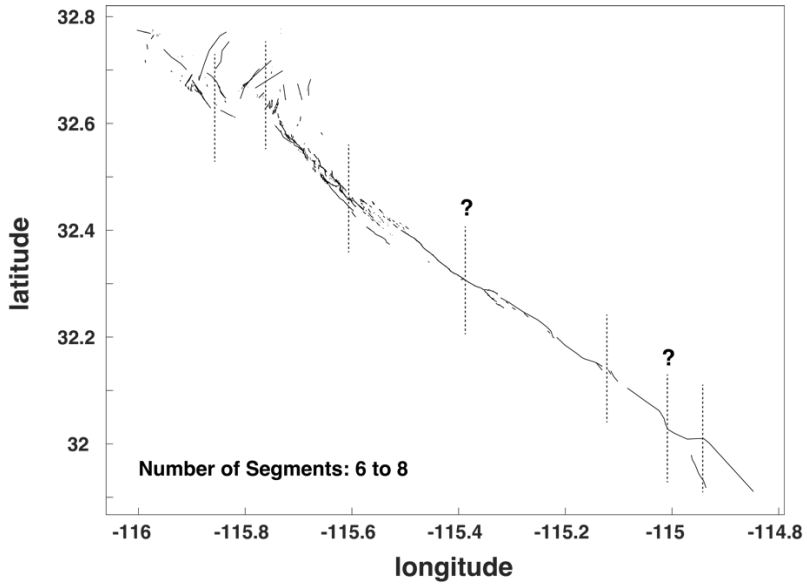

Figure S10. Surface rupture and segmentation results for the El Mayor - Cucapah earthquake.

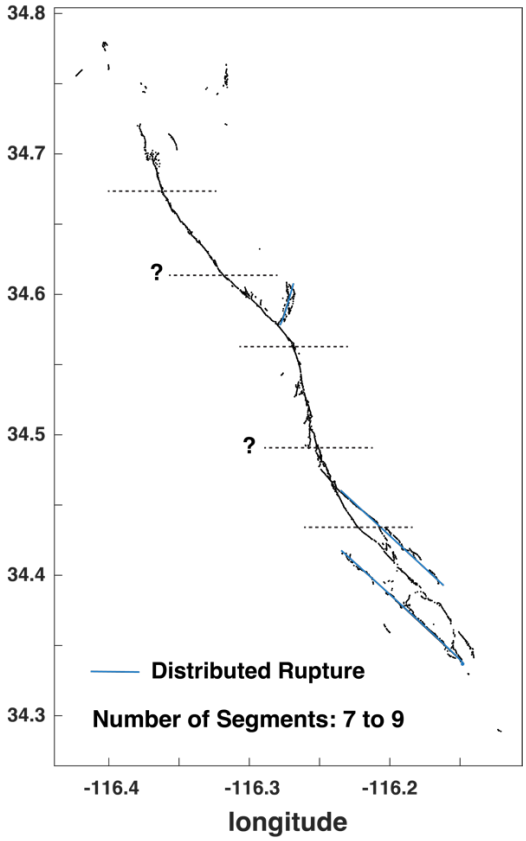

Figure S11. Surface rupture and segmentation results for the Hector Mine earthquake.

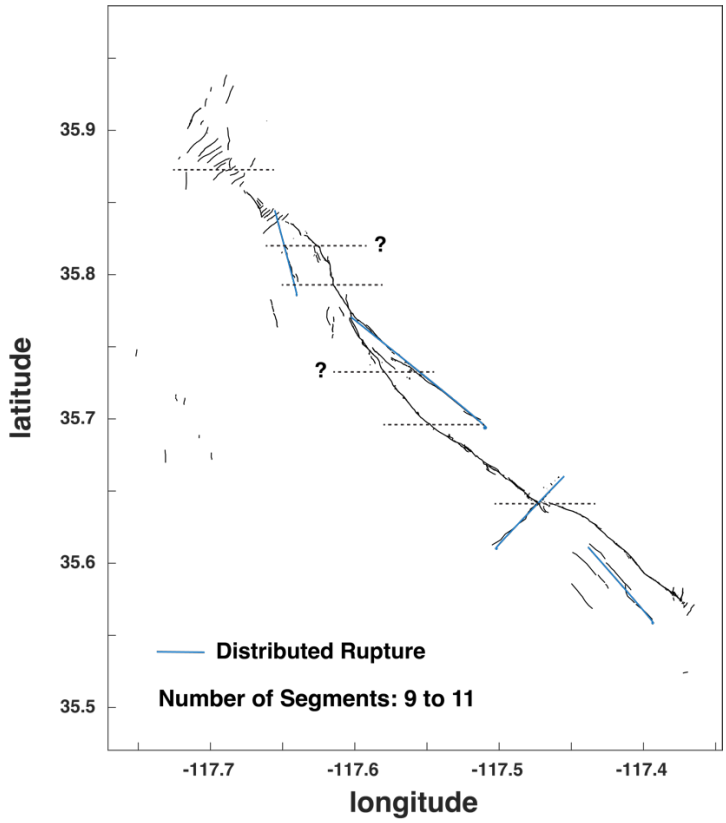

Figure S12. Surface rupture and segmentation results for the Ridgecrest mainshock.

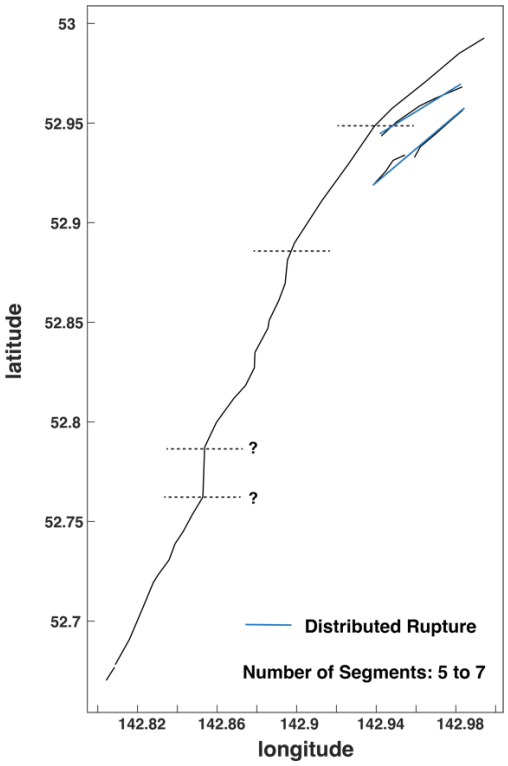

Figure S13. Surface rupture and segmentation results for the Neftegorsk earthquake.

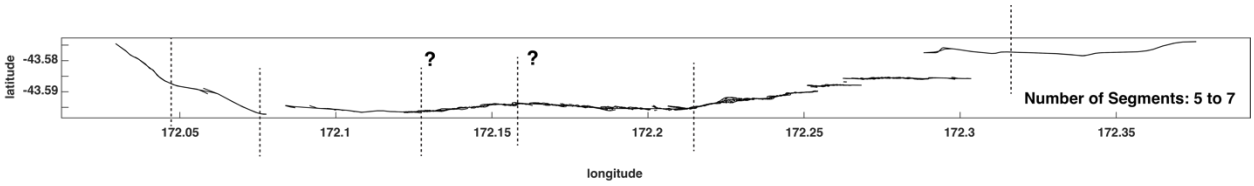

Figure S14. Surface rupture and segmentation results for the Darfield earthquake.

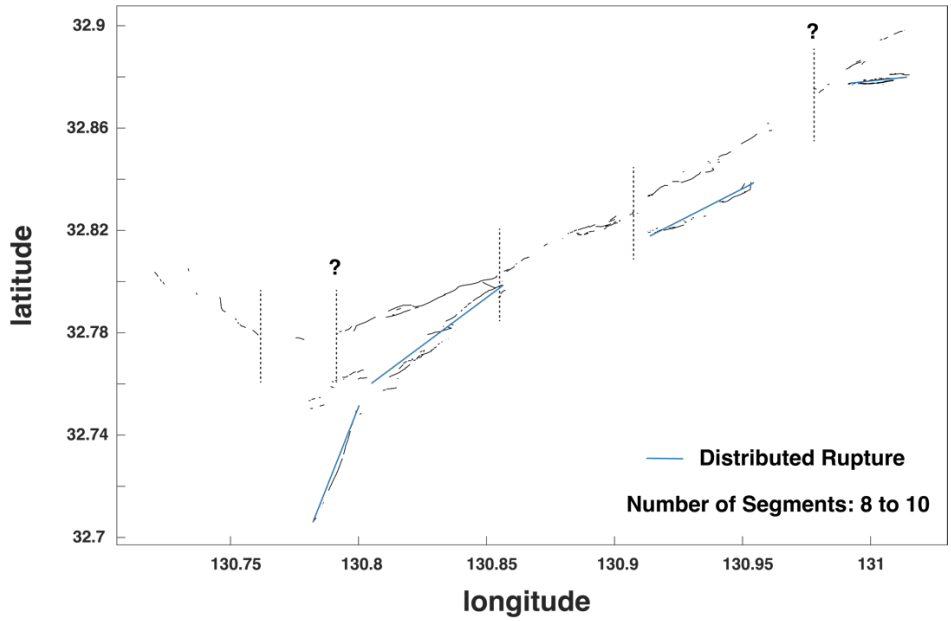

Figure S15. Surface rupture and segmentation results for the Kumamoto earthquake.

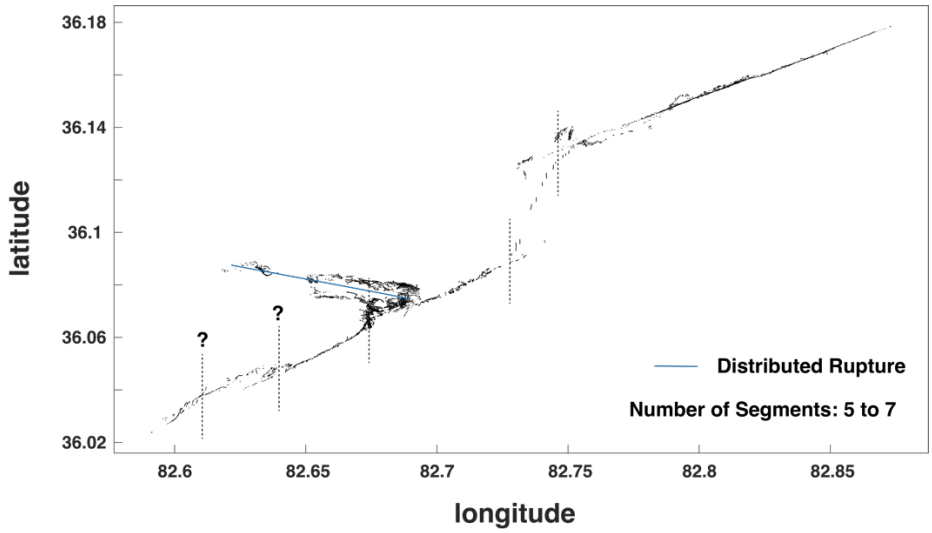

Figure S16. Surface rupture and segmentation results for the Yutian earthquake.

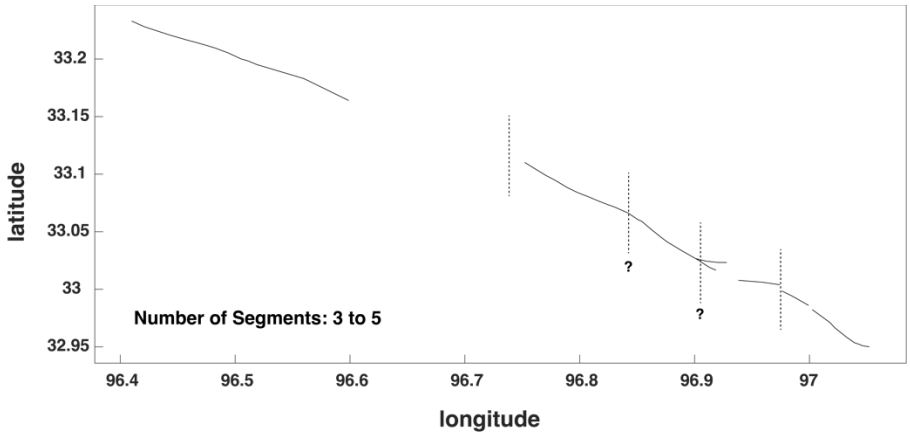

Figure S17. Surface rupture and segmentation results for the Yushu earthquake.

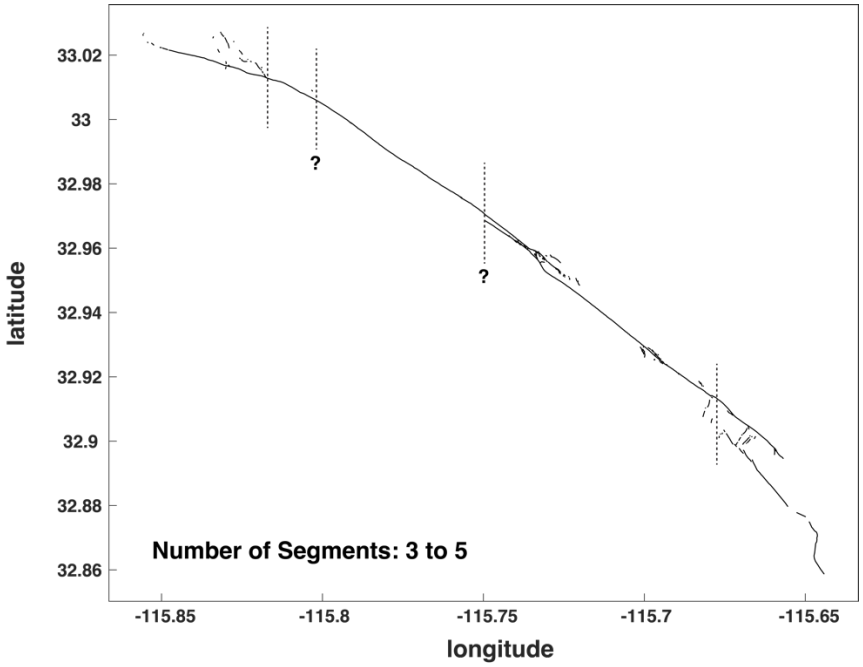

Figure S18. Surface rupture and segmentation results for the Superstition Hills earthquake.

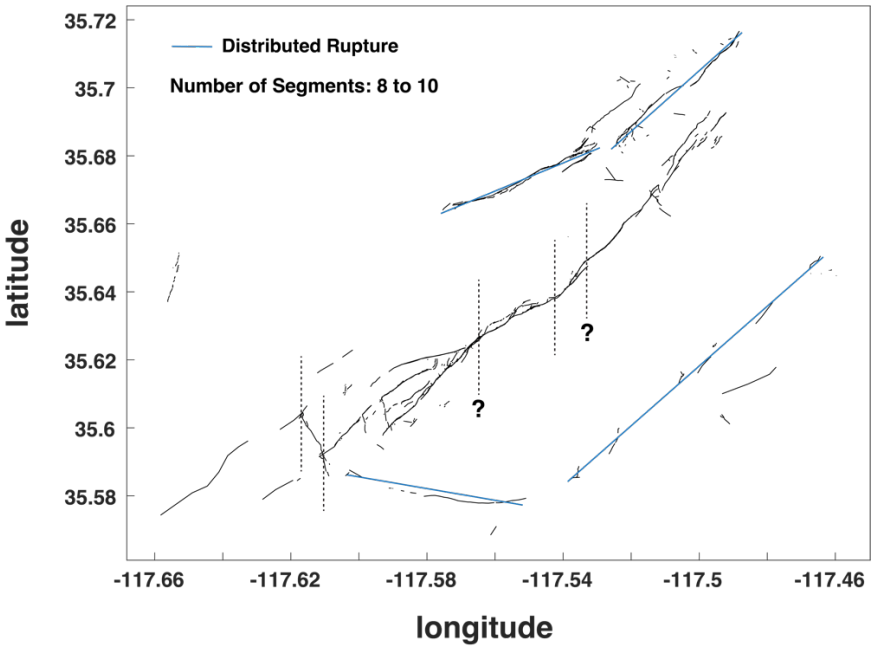

Figure 19. Surface rupture and segmentation results for the Ridgecrest foreshock.

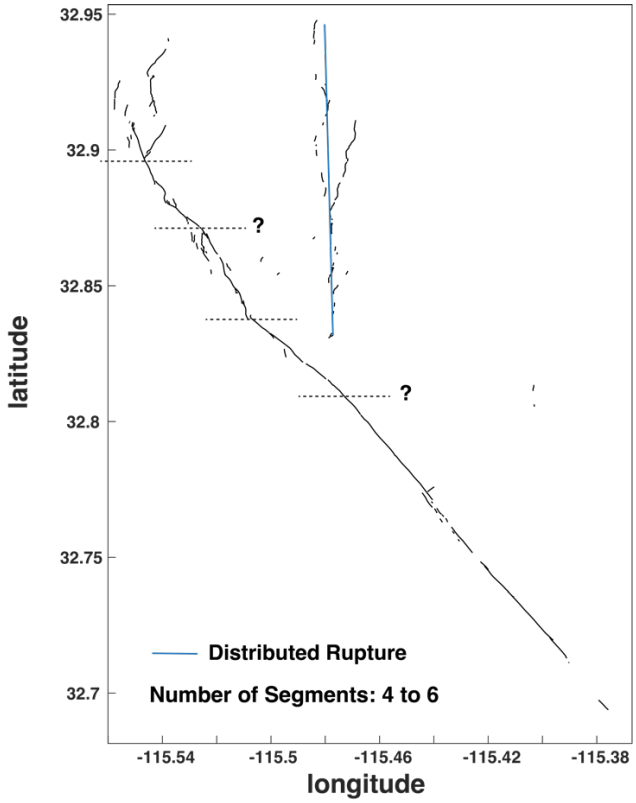

Figure S20. Surface rupture and segmentation results for the Imperial Valley earthquake.

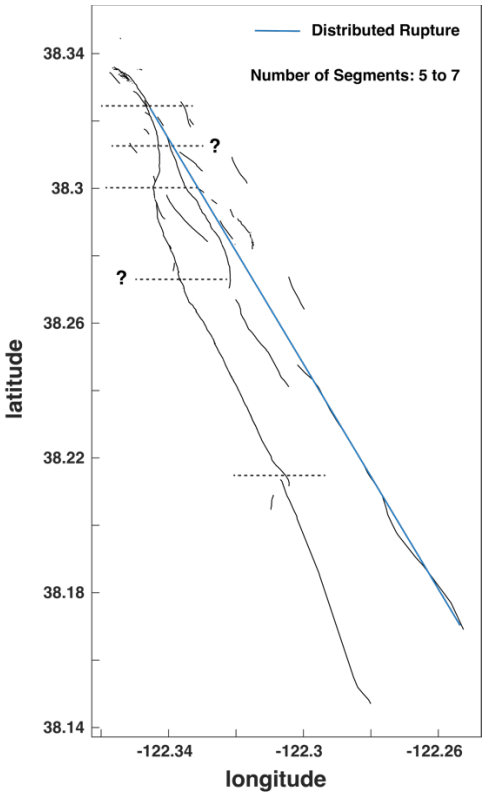

Figure S21. Surface rupture and segmentation results for the Napa earthquake.

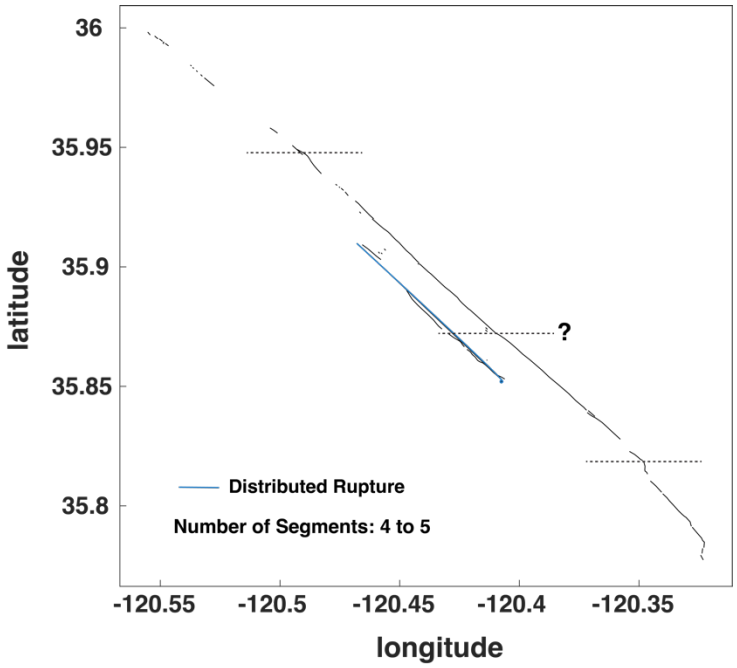

Figure S22. Surface rupture and segmentation results for the Parkfield earthquake.

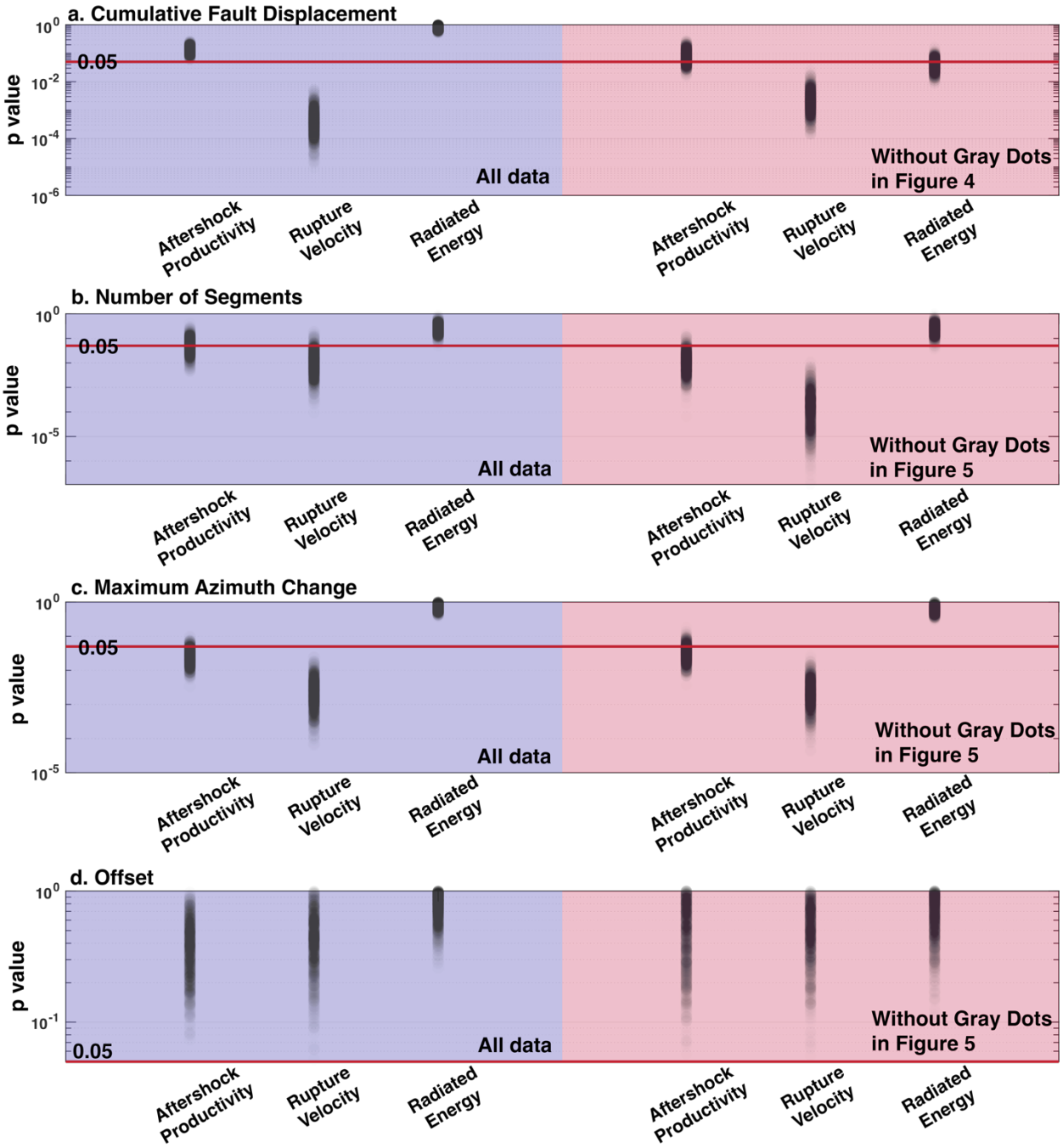

Figure S23. The P-value distributions for bootstrapped comparisons of seismic parameters and a) cumulative fault displacement, b) number of rupture segments, c) maximum change in azimuth between surface rupture traces, and d) stepover offsets between segments.

Supporting Information References

Akbayram, K., Sorlien, C. C., & Okay, A. I. (2016). Evidence for a minimum 52±1km of total offset along the northern branch of the North Anatolian Fault in northwest Turkey. *Tectonophysics*, *668–669*, 35–41. https://doi.org/10.1016/j.tecto.2015.11.026

Ansari, S. (2021). Structural and stress heterogeneities along the 1997 Zirkuh earthquake fault, Eastern Iran. *Bulletin of Engineering Geology and the Environment*, *80*(11), 8319–8337. https://doi.org/10.1007/s10064-021-02436-7

Arefiev, S., Rogozhin, E., Tatevossian, R., Rivera, L., & Cisternas, A. (2000). The Neftegorsk (Sakhalin Island) 1995 earthquake: A rare interplate event. *Geophysical Journal International*, *143*(3), 595–607. https://doi.org/10.1046/j.1365-246X.2000.00234.x

Avouac, J.-P., Ayoub, F., Wei, S., Ampuero, J.-P., Meng, L., Leprince, S., Jolivet, R., Duputel, Z., & Helmberger, D. (2014). The 2013, M_W 7.7 Balochistan earthquake, energetic strike-slip reactivation of a thrust fault. *Earth and Planetary Science Letters*, *391*, 128–134. https://doi.org/10.1016/j.epsl.2014.01.036

Barnhart, W. D., Briggs, R. W., Reitman, N. G., Gold, R. D., & Hayes, G. P. (2015). Evidence for slip partitioning and bimodal slip behavior on a single fault: Surface slip characteristics of the 2013 M_W 7.7 Balochistan, Pakistan earthquake. *Earth and Planetary Science Letters*, *420*, 1–11. https://doi.org/10.1016/j.epsl.2015.03.027

Barrier, E., Huchon, P., & Aurelio, M. (1991). Philippine fault: A key for Philippine kinematics. *Geology*, *19*(1), 32–35. https://doi.org/10.1130/0091-7613(1991)019<0032:PFAKFP>2.3.CO;2

Calais, E., Freed, A., Mattioli, G., Amelung, F., Jónsson, S., Jansma, P., Hong, S.-H., Dixon, T., Prépetit, C., & Momplaisir, R. (2010). Transpressional rupture of an unmapped fault during the 2010 Haiti earthquake. *Nature Geoscience*, *3*(11), Article 11. https://doi.org/10.1038/ngeo992

Çetin, K. Ö., Ilgaç, M., Can, G., Çakır, E., & Söylemez, B. (2020). *Preliminary Report on Engineering and Geological Effects of the January 24, 2020 Magnitude 6.7 Earthquake in Elaziğ, Turkey*. GEER. https://open.metu.edu.tr/handle/11511/95146

Der Woerd, J. V., Tapponnier, P., J. Ryerson, F., Meriaux, A.-S., Meyer, B., Gaudemer, Y., Finkel, R. C., Caffee, M. W., Guoguan, Z., & Zhiqin, X. (2002). Uniform postglacial slip-rate along the central 600 km of the Kunlun Fault (Tibet), from 26Al, 10Be, and 14C dating of riser offsets, and climatic origin of the regional morphology. *Geophysical Journal International*, *148*(3), 356–388. https://doi.org/10.1046/j.1365-246x.2002.01556.x

Duman, T. Y., Emre, O., Dogan, A., & Ozalp, S. (2005). Step-over and bend structures along the 1999 Duzce earthquake surface rupture, North Anatolian Fault, Turkey. *Bulletin of the Seismological Society of America*, *95*(4), 1250–1262. https://doi.org/10.1785/0120040082

Elliott, A., Elliott, J., Hollingsworth, J., Kulikova, G., Parsons, B., & Walker, R. (2020). Satellite imaging of the 2015 *M*7.2 earthquake in the Central Pamir, Tajikistan, elucidates a sequence of

shallow strike-slip ruptures of the Sarez-Karakul fault. *Geophysical Journal International*, *221*(3), 1696–1718. https://doi.org/10.1093/gji/ggaa090

Fialko, Y., Sandwell, D., Simons, M., & Rosen, P. (2005). Three-dimensional deformation caused by the Bam, Iran, earthquake and the origin of shallow slip deficit. *Nature*, *435*(7040), Article 7040. https://doi.org/10.1038/nature03425

Fu, B., Awata, Y., Du, J., Ninomiya, Y., & He, W. (2005). Complex geometry and segmentation of the surface rupture associated with the 14 November 2001 great Kunlun earthquake, northern Tibet, China. *Tectonophysics*, *407*(1), 43–63. https://doi.org/10.1016/j.tecto.2005.07.002

Haeussler, P. J., Schwartz, D. P., Dawson, T. E., Stenner, H. D., Lienkaemper, J. J., Sherrod, B., Cinti, F. R., Montone, P., Craw, P. A., Crone, A. J., & Personius, S. F. (2004). Surface Rupture and Slip Distribution of the Denali and Totschunda Faults in the 3 November 2002 *M* 7.9 Earthquake, Alaska. *Bulletin of the Seismological Society of America*, *94*(6B), S23–S52. https://doi.org/10.1785/0120040626

Jachens, R. C., Langenheim, V. E., & Matti, J. C. (2002). Relationship of the 1999 Hector Mine and 1992 Landers fault ruptures to offsets on Neogene faults and distribution of Late Cenozoic Basins in the Eastern California Shear Zone. *Bulletin of the Seismological Society of America*, *92*(4), 1592–1605. https://doi.org/10.1785/0120000915

Klinger, Y. (2010). Relation between continental strike-slip earthquake segmentation and thickness of the crust. *Journal of Geophysical Research: Solid Earth*, *115*(B7). https://doi.org/10.1029/2009JB006550

Langridge, R. M., Stenner, H. D., Fumal, T. E., Christofferson, S. A., Rockwell, T. K., Hartleb, R. D., Bachhuber, J., & Barka, A. A. (2002). Geometry, slip distribution, and kinematics of surface rupture on the Sakarya Fault segment during the 17 August 1999 İzmit, Turkey, Earthquake. *Bulletin of the Seismological Society of America*, *92*(1), 107–125. https://doi.org/10.1785/0120000804

Li, C., Pang, J., & Zhang, Z. (2012). Characteristics, geometry, and segmentation of the surface rupture associated with the 14 April 2010 Yushu Earthquake, Eastern Tibet, China. *Bulletin of the Seismological Society of America*, *102*(4), 1618–1638. https://doi.org/10.1785/0120110261

Lindsey, E. O., & Fialko, Y. (2016). Geodetic constraints on frictional properties and earthquake hazard in the Imperial Valley, Southern California. *Journal of Geophysical Research: Solid Earth*, *121*(2), 1097–1113. https://doi.org/10.1002/2015JB012516

Maleki Asayesh, B., Zafarani, H., & Tatar, M. (2020). Coulomb stress changes and secondary stress triggering during the 2003 (M_W 6.6) Bam (Iran) earthquake. *Tectonophysics*, *775*, 228304. https://doi.org/10.1016/j.tecto.2019.228304

Marchandon, M., Vergnolle, M., Sudhaus, H., & Cavalié, O. (2018). Fault geometry and slip distribution at depth of the 1997 M_W 7.2 Zirkuh Earthquake: Contribution of near-field displacement data. *Journal of Geophysical Research: Solid Earth*, *123*(2), 1904–1924. https://doi.org/10.1002/2017JB014703

Natawidjaja, D. H., Daryono, M. R., Prasetya, G., Udrekh, Liu, P. L.-F., Hananto, N. D., Kongko, W., Triyoso, W., Puji, A. R., Meilano, I., Gunawan, E., Supendi, P., Pamumpuni, A., Irsyam, M., Faizal, L., Hidayati, S., Sapiie, B., Kusuma, M. A., & Tawil, S. (2021). The 2018 M_W7.5 Palu 'supershear' earthquake ruptures geological fault's multisegment separated by large bends: Results from integrating field measurements, LiDAR, swath bathymetry and seismic-reflection data. *Geophysical Journal International*, *224*(2), 985–1002. https://doi.org/10.1093/gji/ggaa498

Nicol, A., Khajavi, N., Pettinga, J. R., Fenton, C., Stahl, T., Bannister, S., Pedley, K., Hyland-Brook, N., Bushell, T., Hamling, I., Ristau, J., Noble, D., & McColl, S. T. (2018). Preliminary Geometry, displacement, and kinematics of fault ruptures in the epicentral region of the 2016 M_W 7.8 Kaikōura, New Zealand, earthquake. *Bulletin of the Seismological Society of America*, *108*(3B), 1521–1539. https://doi.org/10.1785/0120170329

Okuwaki, R., & Fan, W. (2022). Oblique convergence causes both thrust and strike-slip ruptures during the 2021 *M* 7.2 Haiti earthquake. *Geophysical Research Letters*, *49*(2), e2021GL096373. https://doi.org/10.1029/2021GL096373

Powers, P. M., & Jordan, T. H. (2010). Distribution of seismicity across strike-slip faults in California. *Journal of Geophysical Research: Solid Earth*, *115*(B5). https://doi.org/10.1029/2008JB006234

Quigley, M. C., Jiménez, A., Duffy, B., & King, T. R. (2019). Physical and statistical behavior of multifault earthquakes: Darfield earthquake case study, New Zealand. *Journal of Geophysical Research: Solid Earth*, *124*(5), 4788–4810. https://doi.org/10.1029/2019JB017508

Quigley, M., Dissen, R. V., Litchfield, N., Villamor, P., Duffy, B., Barrell, D., Furlong, K., Stahl, T., Bilderback, E., & Noble, D. (2012). Surface rupture during the 2010 M_W 7.1 Darfield (Canterbury) earthquake: Implications for fault rupture dynamics and seismic-hazard analysis. *Geology*, *40*(1), 55–58. https://doi.org/10.1130/G32528.1

Ren, J., Xu, X., Zhang, G., Wang, Q., Zhang, Z., Gai, H., & Kang, W. (2022). Coseismic surface ruptures, slip distribution, and 3D seismogenic fault for the 2021 M_W 7.3 Maduo earthquake, central Tibetan Plateau, and its tectonic implications. *Tectonophysics*, *827*, 229275. https://doi.org/10.1016/j.tecto.2022.229275

Sangha, S., Peltzer, G., Zhang, A., Meng, L., Liang, C., Lundgren, P., & Fielding, E. (2017). Fault geometry of 2015, M_W 7.2 Murghab, Tajikistan earthquake controls rupture propagation: Insights from InSAR and seismological data. *Earth and Planetary Science Letters*, *462*, 132–141. https://doi.org/10.1016/j.epsl.2017.01.018

Schmidt, J., Hacker, B. R., Ratschbacher, L., Stübner, K., Stearns, M., Kylander-Clark, A., Cottle, J. M., Alexander, A., Webb, G., Gehrels, G., & Minaev, V. (2011). Cenozoic deep crust in the Pamir. *Earth and Planetary Science Letters*, *312*(3), 411–421. https://doi.org/10.1016/j.epsl.2011.10.034

Scott, C., Champenois, J., Klinger, Y., Nissen, E., Maruyama, T., Chiba, T., & Arrowsmith, R. (2019). The 2016 M7 Kumamoto, Japan, earthquake slip field derived from a joint inversion of

differential Lidar topography, optical correlation, and InSAR surface displacements. *Geophysical Research Letters*, *46*(12), 6341–6351. https://doi.org/10.1029/2019GL082202

Socquet, A., Hollingsworth, J., Pathier, E., & Bouchon, M. (2019). Evidence of supershear during the 2018 magnitude 7.5 Palu earthquake from space geodesy. *Nature Geoscience*, *12*(3), Article 3. https://doi.org/10.1038/s41561-018-0296-0

Stirling, M. W., Wesnousky, S. G., & Shimazaki, K. (1996). Fault trace complexity, cumulative slip, and the shape of the magnitude-frequency distribution for strike-slip faults: A global survey. *Geophysical Journal International*, *124*(3), 833–868. https://doi.org/10.1111/j.1365-246X.1996.tb05641.x

Sunal, G., & Erturaç, M. K. (2012). Estimation of the pre-North Anatolian Fault Zone pseudo-paleo-topography: A key to determining the cumulative offset of major post-collisional strike-slip faults. *Geomorphology*, *159–160*, 125–141. https://doi.org/10.1016/j.geomorph.2012.03.013

Treiman, J. A., Kendrick, K. J., Bryant, W. A., Rockwell, T. K., & McGill, S. F. (2002). Primary surface rupture associated with the M_W 7.1 16 October 1999 Hector Mine earthquake, San Bernardino County, California. *Bulletin of the Seismological Society of America*, *92*(4), 1171–1191. https://doi.org/10.1785/0120000923

Valdiya, K. S., & Sanwal, J. (2017). Chapter 4—Mountain arcs and festoons in Pakistan. In K. S. Valdiya & J. Sanwal (Eds.), *Developments in Earth Surface Processes* (Vol. 22, pp. 111–137). Elsevier. https://doi.org/10.1016/B978-0-444-63971-4.00004-9

Walker, R., & Jackson, J. (2004). Active tectonics and late Cenozoic strain distribution in central and eastern Iran. *Tectonics*, *23*(5). https://doi.org/10.1029/2003TC001529

Wang, Y., Lin, Y. N., Simons, M., & Tun, S. T. (2014). Shallow rupture of the 2011 Tarlay earthquake (M_W 6.8), Eastern Myanmar. *Bulletin of the Seismological Society of America*, *104*(6), 2904–2914. https://doi.org/10.1785/0120120364

Yuan, Z., Li, T., Su, P., Sun, H., Ha, G., Guo, P., Chen, G., & Thompson Jobe, J. (2022). Large surface-rupture gaps and low surface fault slip of the 2021 M_W 7.4 Maduo earthquake along a low-activity strike-slip fault, Tibetan Plateau. *Geophysical Research Letters*, *49*(6), e2021GL096874. https://doi.org/10.1029/2021GL096874

Yue, H., Shen, Z.-K., Zhao, Z., Wang, T., Cao, B., Li, Z., Bao, X., Zhao, L., Song, X., Ge, Z., Ren, C., Lu, W., Zhang, Y., Liu-Zeng, J., Wang, M., Huang, Q., Zhou, S., & Xue, L. (2022). Rupture process of the 2021 *M*7.4 Maduo earthquake and implication for deformation mode of the Songpan-Ganzi terrane in Tibetan Plateau. *Proceedings of the National Academy of Sciences*, *119*(23), e2116445119. https://doi.org/10.1073/pnas.2116445119

Zinke, R., Hollingsworth, J., & Dolan, J. F. (2014). Surface slip and off-fault deformation patterns in the 2013 M_W 7.7 Balochistan, Pakistan earthquake: Implications for controls on the distribution of near-surface coseismic slip. *Geochemistry, Geophysics, Geosystems*, *15*(12), 5034–5050. https://doi.org/10.1002/2014GC005538